# Near-Wall Turbulence Models for Complex Flows Including Separation

H. C. Chen* and V. C. Patel†
*The University of Iowa, Iowa City, Iowa*

**Results of a computational experiment designed to investigate the performance of different near-wall treatments in a single turbulence model with a common numerical method are reported. The complete fully elliptic, Reynolds-averaged Navier-Stokes equations have been solved using a low-Reynolds-number model, a new two-layer model, and a two-point wall-function method, in the $k$-$\varepsilon$ turbulence model, for the boundary layer and wake of two axisymmetric bodies. These tests enable the evaluation of the performance of the different approaches in flows involving longitudinal and transverse surface curvatures, streamwise and normal pressure gradients, viscous-inviscid interaction, and separation. The two-layer approach has been found to be quite promising for such flows and can be extended to other complex flows.**

## I. Introduction

THE overall success of all modern turbulence models, in internal as well as external flows, is determined in large measure by the treatment of the boundary conditions at solid walls. The popular wall-function method, which is based on the assumed universality of the law of the wall and the related concept of turbulence in equilibrium, completely avoids the solution of the equations of motion and turbulence model in the wall region. This approach has been utilized in the well known $k$-$\varepsilon$ model, and in the more elaborate Reynolds-stress closure models, even in flows where the continued validity of the underlying physical assumptions becomes questionable. For example, the notion of the law of the wall, and the assumption that all turbulence quantities can be specified in terms of the friction velocity, fail at and beyond separation since the flow in the neighborhood of the wall is no longer controlled by the wall shear stress. Similarly, in three-dimensional flows, the law of the wall provides, at best, only the magnitude of the velocity, leaving its direction to be determined by other means. Quite arbitrary computational expedients have to be introduced to overcome these fundamental problems in the application of wall functions to complex practical flows.

An alternative to the use of wall functions is to employ turbulence models which are valid all the way to the wall. From a critical evaluation of many such "low-Reynolds-number" or "near-wall" extensions of two-equation turbulence models, Patel et al.[1] concluded that none was entirely successful in predicting the essential and well-documented features of the flow close to a solid wall even in the relatively simple case of two-dimensional, attached, steady flows. Their use in more complex flows, therefore, introduces uncertainties in addition to the numerical difficulties of accurately resolving the large gradients of the two-turbulence transport parameters.

Thus, there exists a need for a more general, and yet practical, approach to the problem of accurately resolving the near-wall region in flows involving three dimensionality, unsteadiness, and separation. In the present study, we explore an approach that is intermediate in complexity to the wall function method, on the one hand, and the low-Reynolds-number models, on the other.

Herein, we pursue further the two-layer modeling concept considered by the authors in Ref. 2. There, a simple algebraically prescribed eddy-viscosity model for the wall region was coupled to the $k$-$\varepsilon$ model for the outer flow to describe the details of the flow in the immediate vicinity of the trailing edge of a flat plate. While this approach was quite successful for that particular problem, and could be extended to certain other types of flows, it suffers from the disadvantage that the inner layer is still described in terms of the friction velocity. Consequently, that approach cannot be used for separated flows and cannot be readily extended to unsteady or three-dimensional flows. However, the feasibility of coupling a simple, but more reliable, turbulence model for the flow close to the wall with a more general model for the flow beyond was established. This two-layer approach is also attractive from a practical standpoint. Since the momentum and continuity equations are solved up to the wall, it provides the means to include the complexities noted above without invoking wall functions. Second, the physical uncertainties of near-wall turbulence models and the numerical difficulties of resolving the very large gradients of turbulence parameters are alleviated by reducing the number of turbulence-model equations to be solved in the sublayer and the buffer region.

A general numerical method for the solution of the fully elliptic Reynolds-averaged Navier-Stokes equations, developed by the authors[3,4] is used in conjunction with the low-Reynolds-number and two-layer models to evaluate the relative merits of different treatments of the near-wall flow. In particular, one of the more promising two-equation low-Reynolds-number models identified in Ref. 1, namely that of Lam and Bremhorst,[5] and a two-layer model, which combines the standard $k$-$\varepsilon$ model with the one equation model of Wolfshtein[6] in the near-wall region, are used to calculate unseparated and separated flows over the tail and in the wake of two elongated bodies of revolution for which experimental data were obtained by Huang et al.[7,8] The results are also compared with those obtained with the two-point wall-function method of Chen and Patel.[3]

Received April 6, 1987; presented as Paper 87-1300 at the AIAA 19th Fluid Dynamics, Plasma Dynamics and Laser Conference, Honolulu, HI, June 8–10, 1987; revision received Oct. 7, 1987. 

*Associate Research Scientist, Iowa Institute of Hydraulic Research. Member AIAA.

†Professor of Mechanical Engineering, Iowa Institute of Hydraulic Research. Associate Fellow, AIAA.

## II. Equations and Calculation Method

The details of the general numerical method developed for the solution of three-dimensional turbulent shear flows with a wall-function approach are described in Ref. 3, and its application to the solution of the fully elliptic, Reynolds equations for the flow in the boundary layer and wake of a flat plate is considered in Ref. 2. Consequently, we outline here only the equations and solution procedures as they are adapted for the study of near-wall turbulence models in the flow over axisymmetric bodies.

### Equations

The exact Reynolds-averaged equations of continuity and momentum for unsteady, incompressible axisymmetric mean flow in cylindrical polar coordinates $(x,r,\theta)$ are

$$\frac{\partial U}{\partial x}+\frac{1}{r}\frac{\partial}{\partial r}(rV)=0 \tag{1}$$

$$\frac{\partial U}{\partial t}+U\frac{\partial U}{\partial x}+V\frac{\partial U}{\partial r}+\frac{\partial}{\partial x}(p+\overline{uu})+\frac{\partial}{\partial r}(\overline{uv})+\frac{\overline{uv}}{r}-\frac{1}{R}\nabla^2 U=0 \tag{2}$$

$$\frac{\partial V}{\partial t}+U\frac{\partial V}{\partial x}+V\frac{\partial V}{\partial r}+\frac{\partial}{\partial x}(\overline{uv})+\frac{\partial}{\partial r}(p+\overline{vv})+\frac{1}{r}(\overline{vv}-\overline{ww})-\frac{1}{R}\left(\nabla^2 V-\frac{V}{r^2}\right)=0 \tag{3}$$

where

$$\nabla^2=\frac{\partial^2}{\partial x^2}+\frac{\partial^2}{\partial r^2}+\frac{1}{r}\frac{\partial}{\partial r}$$

$(U,V)$ are the mean velocity components in the $(x,r)$ direction, $(u,v,w)$ are the fluctuating velocity components in the $(x,r,\theta)$ directions, respectively, $t$ is time, $p$ is pressure, and $R=U_oL/\nu$ is the Reynolds number, in which $U_o$ is the freestream velocity, $L$ is the body length, and $\nu$ is the kinematic viscosity. All quantities in the above equations are made dimensionless using $U_o$, $L$ and density $\rho$ in the usual way.

### Turbulence Models

In the present study, the Reynolds stresses are related to the corresponding mean rates of strain through an isotropic eddy-viscosity $\nu_t$,

$$-\overline{uu}=\nu_t\left(2\frac{\partial U}{\partial x}\right)-\frac{2}{3}k \tag{4a}$$

$$-\overline{vv}=\nu_t\left(2\frac{\partial V}{\partial r}\right)-\frac{2}{3}k \tag{4b}$$

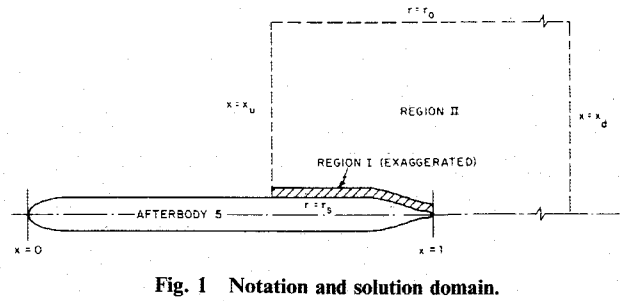


**Fig. 1 Notation and solution domain.**

$$-\overline{ww}=\nu_t\left(2\frac{V}{r}\right)-\frac{2}{3}k \tag{4c}$$

$$-\overline{uv}=\nu_t\left(\frac{\partial U}{\partial r}+\frac{\partial V}{\partial x}\right) \tag{4d}$$

where $k=(\overline{uu}+\overline{vv}+\overline{ww})/2$ is the turbulent kinetic energy. The governing equations (1–3) then become

$$\frac{\partial U}{\partial x}+\frac{1}{r}\frac{\partial}{\partial r}(rV)=0 \tag{5}$$

$$\frac{\partial U}{\partial t}+\left(U-2\frac{\partial \nu_t}{\partial x}\right)\frac{\partial U}{\partial x}+\left(V-\frac{\partial \nu_t}{\partial r}\right)\frac{\partial U}{\partial r}+\frac{\partial p}{\partial x}+\frac{2}{3}\frac{\partial k}{\partial x}-\frac{\partial \nu_t}{\partial r}\frac{\partial V}{\partial x}-\frac{1}{R_U}\nabla^2 U=0 \tag{6}$$

$$\frac{\partial V}{\partial t}+\left(U-\frac{\partial \nu_t}{\partial x}\right)\frac{\partial V}{\partial x}+\left(V-2\frac{\partial \nu_t}{\partial r}\right)\frac{\partial V}{\partial r}+\frac{\partial p}{\partial r}+\frac{2}{3}\frac{\partial k}{\partial r}-\frac{\partial \nu_t}{\partial x}\frac{\partial U}{\partial r}-\frac{1}{R_V}\left(\nabla^2 V-\frac{V}{r^2}\right)=0 \tag{7}$$

where

$$\frac{1}{R_U}=\frac{1}{R_V}=\frac{1}{R}+\nu_t$$

These equations can be solved for $(U,V,p)$ when a suitable turbulence model is employed for the eddy-viscosity distribution. We shall use the $k$-$\varepsilon$ model for this purpose. In this model, $\nu_t$ is related to the turbulent kinetic energy $k$, and its rate of dissipation $\varepsilon$, by

$$\nu_t=C_\mu f_\mu(k^2/\varepsilon) \tag{8}$$

and $k$ and $\varepsilon$ are obtained from the transport equations

$$\frac{\partial k}{\partial t}+\left(U-\frac{1}{\sigma_k}\frac{\partial \nu_t}{\partial x}\right)\frac{\partial k}{\partial x}+\left(V-\frac{1}{\sigma_k}\frac{\partial \nu_t}{\partial r}\right)\frac{\partial k}{\partial r}-\frac{1}{R_k}\nabla^2 k-G+\varepsilon=0 \tag{9}$$

$$\frac{\partial \varepsilon}{\partial t}+\left(U-\frac{1}{\sigma_\varepsilon}\frac{\partial \nu_t}{\partial x}\right)\frac{\partial \varepsilon}{\partial x}+\left(V-\frac{1}{\sigma_\varepsilon}\frac{\partial \nu_t}{\partial r}\right)\frac{\partial \varepsilon}{\partial r}-\frac{1}{R_\varepsilon}\nabla^2\varepsilon-\frac{\varepsilon}{k}(c_{\varepsilon 1}f_1 G-c_{\varepsilon 2}f_2\varepsilon)=0 \tag{10}$$

where

$$\frac{1}{R_k}=\frac{1}{R}+\frac{\nu_t}{\sigma_k},\qquad \frac{1}{R_\varepsilon}=\frac{1}{R}+\frac{\nu_t}{\sigma_\varepsilon}$$

and

$$G=\nu_t\left\{2\left(\frac{\partial U}{\partial x}\right)^2+2\left(\frac{\partial V}{\partial r}\right)^2+2\left(\frac{V}{r}\right)^2+\left(\frac{\partial U}{\partial r}+\frac{\partial V}{\partial x}\right)^2\right\}$$

is the rate of production of $k$, $(C_\mu, C_{\varepsilon 1}, C_{\varepsilon 2}, \sigma_k, \sigma_\varepsilon)$ are constants whose values are (0.09, 1.44, 1.92, 1.0, 1.3), and $f_\mu, f_1$, and $f_2$ are damping functions which are discussed below.

In the wall-function approach, the transport equations [Eqs. (9) and (10)] are solved, with $f_\mu=f_1=f_2=1$, only in the fully turbulent region beyond some distance from the wall. The necessary boundary conditions, namely the velocity components and turbulence parameters, at that distance are usually ob-

tained from a separate analysis of the flow in the sublayer and buffer region using the logarithmic law of the wall and the associated equilibrium relations:

$$\frac{q}{U_\tau} = \frac{1}{\kappa}\ell n y^+ + B \tag{11}$$

$$k = \frac{U_\tau^2}{\sqrt{C_\mu}} \tag{12}$$

$$\varepsilon = (U_\tau^3/\kappa y) \tag{13}$$

where $U_\tau = \sqrt{\tau_w/\rho U_0^2}$ is the friction velocity, $\tau_w$ the wall shear stress, $y^+ = RU_\tau y$, $y$ the normal distance from the wall, $q$ the magnitude of the velocity, $\kappa = 0.418$ the von Karman constant, and $B = 5.45$. The two-point wall-function approach adopted by the authors is somewhat different from the usual practice in two respects. First, following Patel,[9] the effects of pressure gradients on the flow in the wall region are taken into account by the use of a generalized form of the law of the wall,

$$\frac{q}{U_\tau} = \frac{1}{\kappa}\left\{\ell n\left[\frac{4\,(1+\Delta_\tau y^+)^{1/2}-1}{\Delta_\tau\,(1+\Delta_\tau y^+)^{1/2}+1}\right]\right.$$

$$\left. +2[(1+\Delta_\tau y^+)^{1/2}-1] + B + 3.7\Delta_p\right. \tag{14}$$

in which $\Delta_p = \nabla p/(RU_\tau^3)$ is a pressure-gradient parameter and $\Delta_\tau$ is a similar stress-gradient parameter which is assumed to be $0.5\Delta_p$. Second, we ensure that the first two near-wall grid points lie within the fully turbulent layer and explicitly satisfy Eq. (14) at both. An iterative solution of this equation then provides the values of $U_\tau$ and $q$, required to establish the boundary conditions, without any analysis of the flow in the sublayer and the buffer region. Further details of this two-point wall-function method are given in Refs. 2 and 3.

While the wall-function method has been found to be quite satisfactory for a range of attached two-dimensional and axisymmetric flows, it is not suitable for separated flow and its extension to three-dimensional and unsteady flows requires additional assumptions which are not substantiated by experiment or theory. For all such cases, therefore, it is necessary to resolve the flow all the way to the wall. Patel et al.[1] have reviewed and evaluated several such near-wall, or low-Reynolds-number, extensions of two-equation turbulence models within the context of steady, two dimensional boundary layers in pressure gradients. Most of these are based on the $k$-$\varepsilon$ model and differ from one another in the damping functions $f_\mu$, $f_1$ and $f_2$ introduced in Eqs. (9) and (10).

In the present study, we have selected one of the more successful of these models, namely that of Lam and Bremhorst,[5] to examine its performance in the prediction of separation and separated flows, and to compare it with a simpler alternative. The damping functions in this model are

$$f_\mu = [1-\exp(-0.0160\,R_y)]^2\left(1+\frac{19.5}{R_T}\right) \tag{15a}$$

$$f_1 = 1+(0.06/f_\mu)^3 \tag{15b}$$

$$f_2 = 1-\exp(-R_T^2) \tag{15c}$$

where $R_y$ and $R_T$ are the turbulence Reynolds numbers

$$R_y = R\sqrt{k}y, \qquad R_T = Rk^2/\varepsilon \tag{16}$$

The constants in Eqs. (15) are somewhat different from those quoted by Lam and Bremhorst, the values used here being those recommended by Rodi et al.[10] It is noted that two of the damping functions depend explicitly upon the normal distance $y$ from the wall. This is obviously not appropriate for describing the gradual destruction of the sublayer in the near wake. In order to model correctly the transition from a near-wall sublayer to a fully turbulent wake, the damping functions need to be restored gradually to unity through the very near wake. While we recognize this subtlety, we note that the resolution of the linear inner wake is not particularly critical in the cases treated here, and, therefore, we simply assume that the flow becomes fully turbulent in the wake and set $f_\mu = f_1 = f_2 = 1$.

As an alternative to the low-Reynolds-number turbulence models of the type described above, we consider a two-layer model which combines the standard $k$-$\varepsilon$ model with a simpler, but more reliable one-equation model to resolve accurately the flow near a solid wall. In this approach, the flow domain is divided into two regions as shown in Fig. 1. Region I includes the sublayer, the buffer layer, and a part of the fully turbulent layer. The one-equation model of Wolfshtein[6] is employed in this region to account for the wall proximity effects, whereas the standard $k$-$\varepsilon$ model is used in region II. Unlike the low-Reynolds-number models that require the solution of the transport equations of both $k$ and $\varepsilon$ all the way to the wall, the one-equation model requires the solution of only the turbulent kinetic energy equation in region I. The rate of energy dissipation in this region is specified by

$$\varepsilon = (k^{3/2}/\ell_\varepsilon) \tag{17}$$

where the eddy-viscosity is obtained from

$$\nu_t = C_\mu\sqrt{k}\,\ell_\mu \tag{18}$$

where the length scales $\ell_\mu$ and $\ell_\varepsilon$ contain the necessary damping effects in the near-wall region in terms of the turbulence Reynolds number $R_y$:

$$\ell_\mu = C_\ell y\,[1-\exp(-R_y/A_\mu)] \tag{19a}$$

$$\ell_\varepsilon = C_\ell y[1-\exp(-R_y/A_\varepsilon)] \tag{19b}$$

Note that both $\ell_\mu$ and $\ell_\varepsilon$ become linear, and approach $C_\ell y$, with increasing distance from the wall. In the present study, $C_\ell$ is given by

$$C_\ell = \kappa C_\mu^{-3/4} \tag{20}$$

to ensure a smooth eddy-viscosity distribution at the junction of regions I and II. In addition, $A_\varepsilon = 2C_\ell$ is assigned so as to recover the proper asymptotic behavior

$$\varepsilon = (2\nu k/y^2) \tag{21}$$

in the sublayer. The third parameter, $A_\mu = 70$, is determined from numerical tests to recover the additive constant, $B = 5.45$, in the logarithmic law in the case of a flat plate boundary layer. In view of the above procedures, these constants are somewhat different from those reported in Wolfshtein[6] and Launder.[11] In region II, beyond the near-wall layer, the standard $k$-$\varepsilon$ model is employed to calculate the velocity field as well as the eddy viscosity. As noted earlier, the standard model represents a special case in which the three damping functions are set equal to unity.

It should be remarked here that the two turbulence Reynolds number $R_y$ and $R_T$ depend only on the local turbulence intensity. In particular, the wall shear stress $\tau_w$ is not involved. Both $R_y$ and $R_T$ vary relatively slowly along lines parallel to the wall ($y$ = const), do not vanish at separation, and remain well-defined in regions of flow reversal. Consequently, the damping effects decay rapidly with distance from the wall regardless of the magnitude of the wall shear stress. Because the damping effect is confined to the near-wall region, the matching between the one-equation and the standard $k$-$\varepsilon$ models in the two-layer approach can be carried out along preselected grid lines, even for complex flows involving separation. In the present applications, the match boundary is chosen along a grid line where the

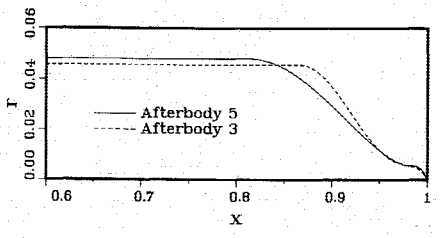


**Fig. 2 Tail geometry of the bodies.**

minimum $R_y$ is of the order of 250, so that the damping effects are negligible. This ensures a smooth eddy-viscosity distribution across the match boundary. Several other match boundaries were also tested, and the results were found to be insensitive to their location, provided the minimum value of $R_y$ was greater than 200.

### Coordinates and Numerical Grid

The governing equations are transformed into numerical coordinates $(\xi,\eta)$ which are defined by the two Poisson equations

$$\nabla^2\xi = f^1$$
$$\nabla^2\eta = f^2 \tag{22}$$

where $f^1$ and $f^2$ are grid-control functions selected to obtain a desired distribution of grid points in the physical $(x,r)$ space. In the present calculations, these functions were determined by the specified boundary node distributions. The numerical grid is generated by the solution of the inverted forms of Eq. (22), i.e.,

$$g^{11}x_{\xi\xi} + g^{22}x_{\eta\eta} + 2g^{12}x_{\xi\eta} + f^1x_\xi + f^2x_\eta = 0$$
$$g^{11}r_{\xi\xi} + g^{22}r_{\eta\eta} + 2g^{12}r_{\xi\eta} + f^1r_\xi + f^2r_\eta = \frac{1}{r} \tag{23}$$

where

$$g^{11} = r^2(x_\eta^2 + r_\eta^2)/g$$
$$g^{22} = r^2(x_\xi^2 + r_\xi^2)/g$$
$$g^{12} = -r^2(x_\xi x_\eta + r_\xi r_\eta)/g$$
$$g = r^2(x_\xi r_\eta - x_\eta r_\xi)^2$$

In the numerical coordinates, the continuity equation becomes

$$(1/J)[(b_1^1U + b_2^1V)_\xi + (b_1^2U + b_2^2V)_\eta] = 0 \tag{24}$$

and the transport equations of momentum [Eqs. (6) and (7)] and turbulence [Eqs. (9) and (10)] can be written in the form

$$g^{11}\phi_{\xi\xi} + g^{22}\phi_{\eta\eta} = 2A_\phi\phi_\xi + 2B_\phi\phi_\eta + R_\phi\phi_t + S_\phi \tag{25}$$

where $\phi = U,V,k,\varepsilon$. The Jacobian $J$ of the transformation, the associated geometric coefficients $b_i^j$, the coefficients $A_\phi$, and $B_\phi$, and the source functions $S_\phi$ are all given in Ref. 3.

### Numerical Techniques

The grid-generation equation [Eq. (23)] is solved by an exponential finite-difference scheme. The four transport equations (25) are solved by the finite-analytic scheme. In this latter approach, Eq. (25) is first linearized in each local element ($\Delta\xi = \Delta\eta = 1$) by evaluating the coefficients $A_\phi$ and $B_\phi$ at an interior node point $P$. The resulting linear equation is then

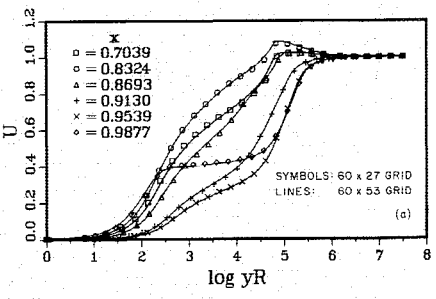


**a) Velocity profiles**

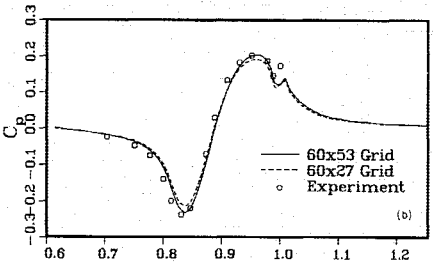


**b) Pressure distribution**

**Fig. 3 Grid dependence with two-layer model.**

solved analytically by the method of separation of variables. The boundary conditions required in this solution are expressed as combinations of linear and exponential functions involving the unknown nodal values. Evaluation of the analytic solutions at the interior node then provides a 10-point discretization formula of the form

$$\phi_p = \frac{1}{1 + C_p(R_\phi/\tau)}\Big\{C_{EC}\phi_{EC} + C_{WC}\phi_{WB} + C_{NC}\phi_{NC} + C_{SC}\phi_{SC} + C_{NE}\phi_{NE} + C_{NW}\phi_{NW} + C_{SE}\phi_{SE} + C_{SW}\phi_{SW} + C_p(R_\phi/\tau)\phi_p^{n-1} - C_p(S_\phi)_p\Big\} \tag{26}$$

where

$$e^{Ah}C_{EC} = e^{-Ah}C_{WC} = P_B/(2\cosh Ah)$$
$$e^{Bk}C_{NC} = e^{-Bk}C_{SC} = P_A/(2\cosh Bk)$$
$$e^{Ah+Bk}C_{NE} = e^{-Ah+Bk}C_{NW} = e^{Ah-Bk}C_{SE}$$
$$= e^{-Ah-Bk}C_{SW} = (1 - P_A - P_B)/(4\cosh Ah\cosh Bk)$$
$$C_p = h(1 - P_A)/(2A\coth Ah)$$
$$= k(1 - P_B)/(2B\coth Bk)$$
$$P_A = 4Ah\cosh Ah\cosh Bk\coth Ah \times \sum_{m=1}^{\infty}\frac{-(-1)^m\lambda_m h}{[(Ah)^2 + (\lambda_m h)^2]^2\cosh\sqrt{A^2 + B^2 + \lambda_m^2}k}$$
$$P_B = 1 + \frac{Bh\coth Bk}{Ak\coth Ah}(P_A - 1)$$
$$\lambda_m h = \left(m - \frac{1}{2}\right)\pi$$
$$A = \frac{(A_\phi)_p}{\sqrt{g_p^{11}}},\quad B = \frac{(B_\phi)_p}{\sqrt{g_p^{22}}},\quad h = \frac{1}{\sqrt{g_p^{11}}},\quad k = \frac{1}{\sqrt{g_p^{22}}}$$

the subscripts denote east-central (EC), northeast (NE), etc., $\tau$ the time step, and the superscript $(n-1)$ denotes the values at

the previous time step. For large-cell Reynolds number $Ah$ and/or $Bk$, the series summation for $P_A$ can be avoided by the following asymptotic expressions:

$Ak \coth Ah \geq Bh \coth Bk$:

$$P_A = 0, P_B = 1 - (Bh \coth Bk)/(Ak \coth Ah) \quad (27a)$$

$Ak \coth Ah < Bh \coth Bk$:

$$P_B = 0, P_A = 1 - (Ak \coth Ah)/(Bh \coth Bk) \quad (27b)$$

Equation (26) is employed to solve the transport equation, Eq. (25), assuming that the pressure field is known. The pressure is then updated by a two-step, global pressure-solution procedure, similar to the SIMPLER algorithm of Patankar,[12] which ensures the satisfaction of the equation of continuity.[24] As noted earlier, details of the numerical method are given in Ref. 3.

## III. Results and Discussion

Calculations have been performed for several different axisymmetric bodies for which detailed experimental data are available. Here, however, we shall present the results for only two cases, namely afterbody 5 and afterbody 3 tested by Huang et al.[7,8] to illustrate the performance of the different near-wall treatments. The two bodies have the same parallel middle body and a streamlined forebody, as shown in Fig. 1, but the model with afterbody 3 has a longer total length. Figure 2 shows the two afterbodies. It is seen that both contain points of inflection and quite dramatic changes in surface curvature. These induce strong favorable and adverse pressure gradients over the stern and in the region of the propeller hub. In the case of afterbody 3, the pressure gradients are such as to lead to a small separation bubble around the inflection point. Together, the two cases enable us to evaluate the general performance of the different near-wall treatments with the same turbulence model in flows involving large longitudinal and transverse curvatures, strong pressure gradients associated with these curvatures, and a separation bubble.

### Attached Turbulent Flow: Afterbody 5

The calculations with the low-Reynolds-number and the two-layer models for afterbody 5 were performed at the experimental Reynolds number of $R = 9.3 \times 10^6$. Sixty axial stations were used in the domain $0.6 < x < 13.20$, where $x$ is measured along the axis of the body from the nose. In the radial direction, 27 points were used between the body surface $r = r_s$ and the external boundary $r = r_o = 3.48$ (see Fig. 1). The match boundary for the two-layer model was located along the grid line $\eta = 12$, and the first grid node ($\eta = 2$) was located in the sublayer at $y^+ \sim 0.2$. In the calculations using the two-point wall-function approach, a $60 \times 18$ grid, obtained simply by deleting the innermost nine radial grid lines of the previous case, was employed. In this case, the first grid line was located at $y^+$ values ranging from 60 to 100. For simplicity, standard flat-plate boundary-layer profiles were specified at the upstream station $x = 0.6$ for all calculations. The calculations using the two-layer and wall-function approaches were started with an initial condition of zero pressure everywhere, the initial conditions for velocity and turbulence quantities being obtained by a parabolic marching technique, similar to that described in Ref. 3. In the two-layer calculations, satisfactory convergence was obtained in less than 300 time steps, and the complete calculation with 300 steps took about 30 min of CPU time on a Prime 9950 minicomputer. For the low-Reynolds-number approach, calculations were started with the final two-layer solutions to accelerate the convergence and save computing time. Fully converged solutions were obtained in about 100 iterations, which took an additional 10 min of CPU time.

Grid dependence of the solutions with the two-layer model was examined by doubling the grid nodes in the radial direction to $60 \times 53$. From Fig. 3 it is seen that the velocity profiles are fairly insensitive, but the pressure distribution is in somewhat better agreement with experiment after grid refinement. All subsequent results were obtained with the coarser grid.

Figure 4 shows the calculated and measured velocity and turbulent kinetic-energy profiles at three representative axial stations. It is clear that all three approaches yield a nearly identical mean-velocity field due, presumably, to the use of the same turbulence model for the flow outside the near-wall region. The calculated turbulent kinetic energy, however, is somewhat more sensitive to the near-wall treatment. The relative insensitivity of the pressure distribution, shown in Fig. 5, is to be expected because of the insensitivity of the mean-velocity field. The small differences that are observed are related to the different distributions of the normal stress $\overline{vv}$ implied by the different near-wall treatments, as was discussed in detail in Ref. 2.

Figure 6 shows the calculated and measured friction velocities $U_\tau$. In order to understand these results, it is important to note the different ways in which the wall shear stress, and therefore, $U_\tau$, was determined. In the calculations with the low-Reynolds-number and two-layer models, $U_\tau$ was determined directly from the velocity gradient at the wall. On the other hand, in the wall-function method, it is determined by ensuring that Eq. (14) is satisfied at two grid points placed in the fully turbulent layer. In the experiments, which employed Clauser plots and Preston tubes, the validity of the usual logarithmic law of the wall, without pressure gradient corrections, Eq. (11), is assumed. While the differences in $U_\tau$ shown in Fig. 6 appear to be large and somewhat surprising, they can best be understood by examining the near-wall velocity distributions without reference to the wall shear stress. This is accomplished by plotting the experimental and calculated velocity profiles in the format of the Clauser plot ($U$ vs $\log y$). These are shown in Fig. 7. Also included are some lines determined from Eq. (11), with $U_\tau$ as a parameter. Conformity of a calculated or experimental profile with these parametric lines in some portion of the near-wall region indicates the validity of the logarithmic law. Figure 7 thus provides detailed insights into the results.

We again note that all three calculations give essentially the same velocity distribution beyond some distance from the wall.

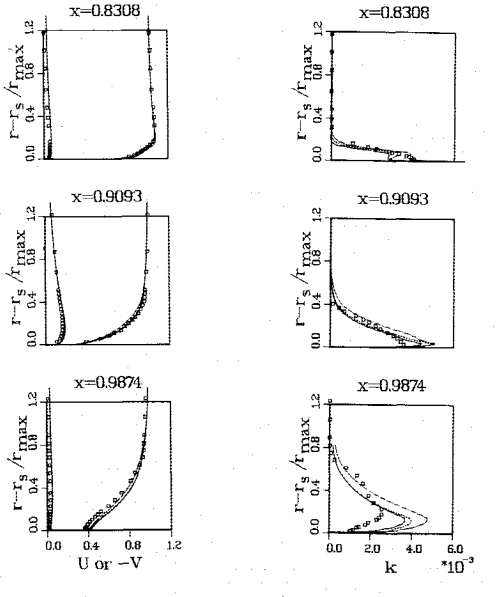


**Fig. 4 Velocity and turbulent energy profiles, afterbody 5. Symbols, Experiment (7): ———, two-layer model; – – –, low *Re* model; . . . . . , wall functions.**

The calculations with wall functions appear to be in agreement with the data even in the very thick boundary layer over the propeller hub ($x = 0.9874$). However, the fact that these calculations also provide the best agreement with the "experimental" $U_\tau$ in Fig. 6 is not particularly surprising because both the calculations and experiments use the same empirical information. Indeed, a closer examination of the measured velocity profiles at the two downstream stations reveals that they are not sufficiently detailed in the wall region to provide unmistakable evidence in support of the wall-function method. If the velocity profiles calculated with the two near-wall models were to be analyzed on the basis of the Clauser plots, it is clear that they would also yield values of $U_\tau$ in substantial agreement with the "experimental" ones.

It should be noted here that in the present wall-function method, Eq. (14) was employed only in regions of adverse pressure gradients, and it is, at best, a local equilibrium approximation, i.e., it does not take account of any history effects. Its use in favorable pressure gradients is rather restrictive, because, for even moderate pressure gradients, the required correction becomes unrealistically large (giving negative argument of the logarithmic term) at $y^+$ values which are too small to be justified in a wall-function approach. In other words, we conclude that the use of wall functions in flows with moderate to strong favorable pressure gradients is questionable. It is also of interest to note here that replacement of Eq. (14) by Eq. (11) in the wall-function method in general leads to higher wall shear stresses in adverse pressure gradients and poorer overall agreement with experiments. This further justifies the need for a pressure-gradient correction in the wall layer, and in fact the need to abandon the wall-function approach altogether for complex flows.

Figure 7 shows that the calculations with the low-Reynolds-number model and the two-layer approach are in agreement everywhere except in the buffer layer between the sublayer and the fully turbulent region. The shear stresses calculated from the velocity gradients at the wall are also quite close except that the two-layer model yields values closer to those determined from wall functions in the region of adverse pressure gradients ($0.83 < x < 0.94$). The velocity distributions predicted with both near-wall treatments show a strong influence of pressure gradient in the wall region, and an eventual breakdown of the law of the wall. For example, the shape of the profile at $x = 0.8308$ indicates an influence of the favorable pressure gradient that existed upstream, that at $x = 0.9093$ shows the effects of the adverse pressure gradient, while that at $x = 0.9874$ shows no logarithmic layer at all.

Finally, the results of the two-layer model are plotted in the conventional inner-layer coordinates in Fig. 8, with $U_\tau$ determined from the velocity gradient at the wall as the normalizing parameter. This format provides a confirmation of the ability of this near-wall turbulence model to reproduce the well-documented universality of the near wall velocity distribution in small pressure gradients. When the results of the low-Reynolds-number model are plotted in a similar format, there is considerable scatter, indicating that it is not entirely consistent with experimental evidence. Figure 8 shows that the velocity profiles predicted with the two-layer model deviate gradually from the logarithmic line, upward in adverse pressure gradients, and downward in favorable pressure gradients, consistent with the type of equilibrium analysis which leads to Eq. (14). Figure 8 also shows the breakdown of the logarithmic region beyond $x = 0.963$ and, eventually, the destruction of the buffer layer and sublayer in the neighborhood of the tail of the body. The calculations in the near wake are qualitatively similar to those for the flat plate discussed in Ref. 2 with regard to

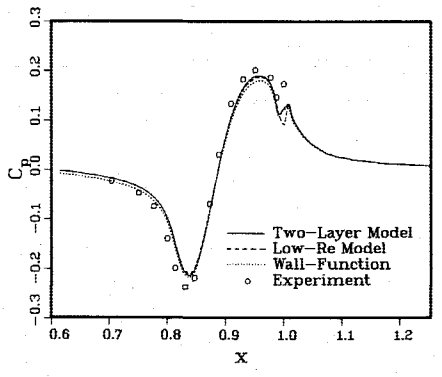


**Fig. 5 Pressure distribution, afterbody 5.**

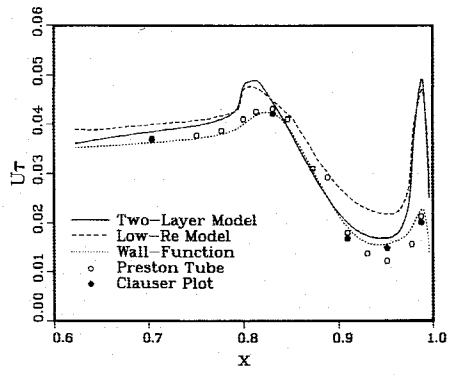


**Fig. 6 Friction velocity, afterbody 5.**

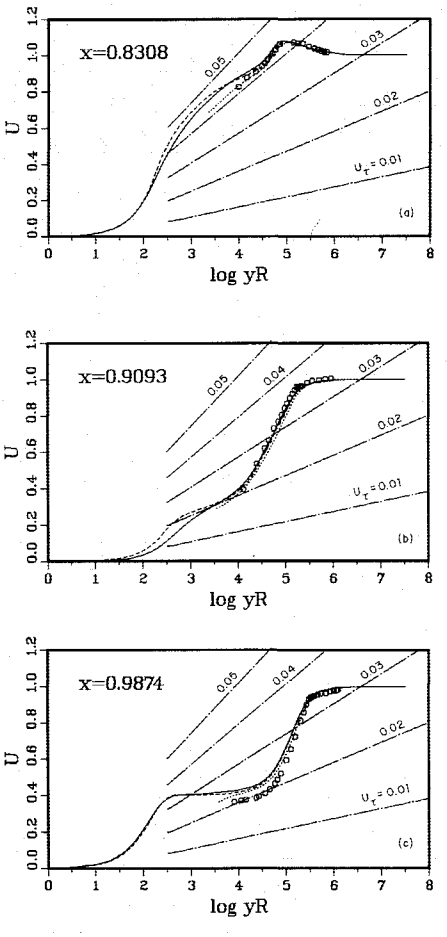


**Fig. 7 Velocity profiles in Clauser charts, afterbody 5: o, Experiment (7); ———, two-layer model; -----, low *Re* model; . . . . . , wall functions; — . —, Eq. (11).**

the gradual erosion of the wall layer and the development toward an asymptotic state.

From the results presented in Figs. 4–8, it would appear that the present two-point wall-function method with pressure-gradient corrections as well as the proposed two-layer model account for pressure gradient effects somewhat better than the low-Reynolds-number model of Lam and Bremhorst. This observation is similar to that made recently by Rodi and Scheuerer[13] on the basis of solutions of the boundary-layer equations in adverse pressure gradients.

Further comparisons between the low-Reynolds-number model and the two-layer model are provided by the next example, which involves a separation bubble. The wall-function approach could not be used in this case at least without further approximations for reasons already discussed.

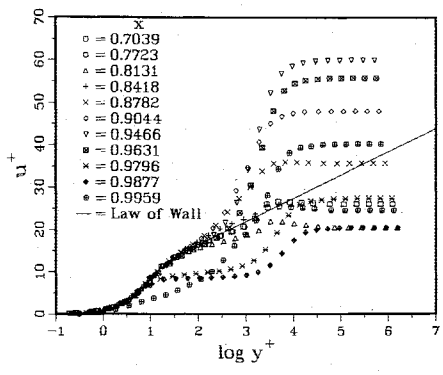


**Fig. 8 Velocity profiles in wall coordinates.**

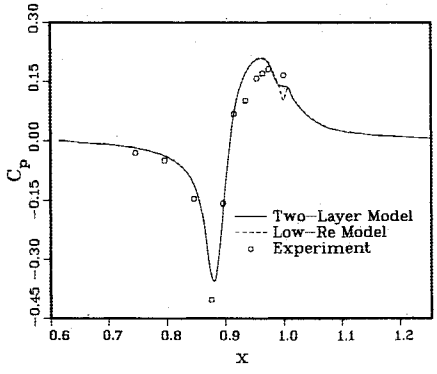


**Fig. 9 Pressure distribution, afterbody 5.**

**S: Experimental separation**
**R: Experimental reattachment**

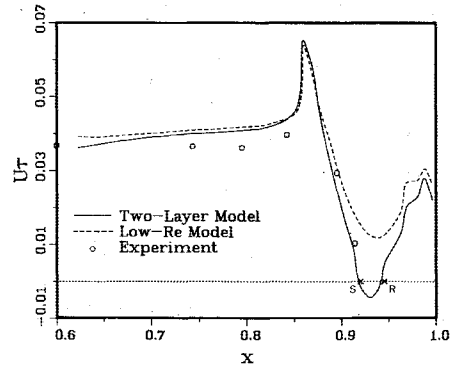


**Fig. 10 Friction velocity, afterbody 3.**

**Turbulent Flow with Separation: Afterbody 3**

As noted earlier, afterbody 3 (shown in Fig. 2) was chosen to test the performance of the near-wall models in a flow involving separation. This case was favored over the ubiquitous two-dimensional, backward- and forward-facing steps because it involves the prediction of the location of separation as well as reattachment, and questions concerning two-dimensionality of the data are not as critical. The calculations for afterbody 3 were carried out in a manner entirely similar to that for the previous case. In particular, the size of the solution domain, the number of grid points, and the initial and boundary conditions were all comparable. The results are presented in Figs. 9–12 also in a similar format. We shall discuss only the most important features here.

Figure 9 shows that the pressure distribution is again insensitive to the near-wall treatment over most of the body surface and in the wake, and both models yield reasonably good agreement with experiment. There exists a very small difference between the results of the two calculations at the tail of the body. A similar difference is also seen in the previous case (Fig. 5). For the purposes of the present paper, it suffices to note that this difference stems from the manner in which the source terms in the turbulence-model equations are treated in the numerical cell surrounding the tail itself.

Figure 10 reveals that the wall shear stresses, obtained from the velocity gradients at the wall with both models, differ considerably in the region of adverse pressure gradients, as was also observed in the previous test case. In fact, the low-Reynolds-number model of Lam and Bremhorst predicts no separation, whereas the two-layer model accurately predicts the locations of separation as well as reattachment that were observed with flow visualizations in the experiment. The velocity profiles plotted in Fig. 11 in the usual format show practically no difference between the two solutions. However, from the Clauser plots of Fig 12, it is clear that the two models give very different velocity distributions in the sublayer and the buffer layer. The low-Reynolds-number model predicts much higher velocities in these regions. Although the experimental evidence is not conclusive, Figs. 12c and 7c suggest that even the two-layer model tends to overestimate the velocities in the inner layer, indicating a reduction in the turbulence length scale. Further tests are required to study the origin of this behavior.

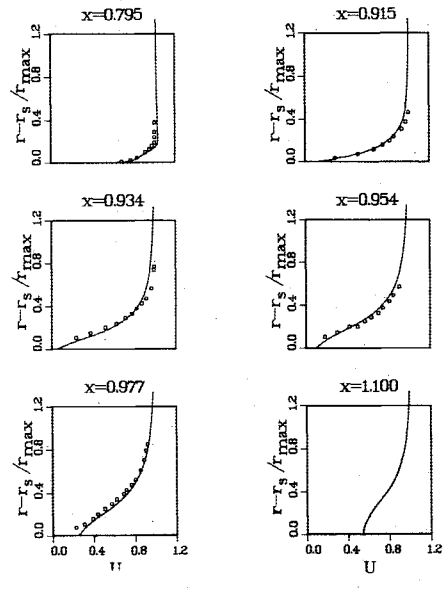


**Fig. 11 Axial velocity profiles, afterbody 3: ○, Experiment (8); ———, two-layer model; -----, low *Re* model.**

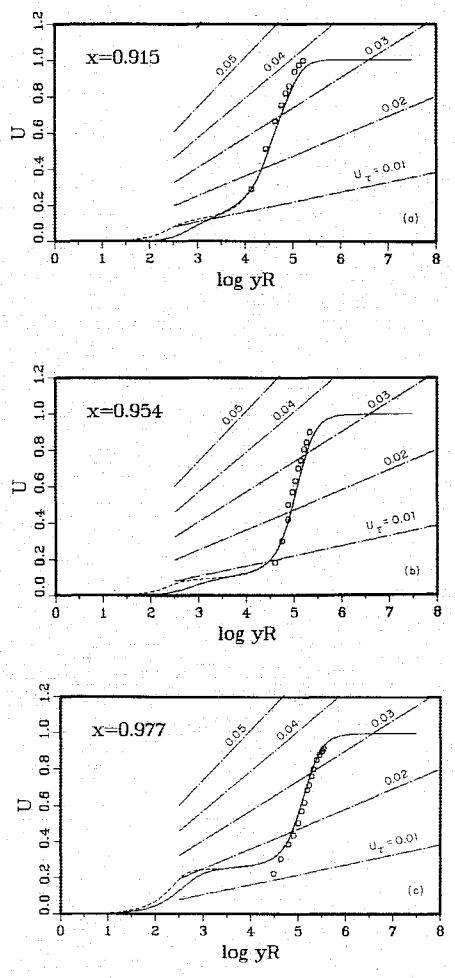


**Fig. 12 Velocity profiles in Clauser charts, afterbody 3: o, Experiment (8); — . —, Eq. (11); ———, two-layer model; -----, low *Re* model.**

## Concluding Remarks

A general numerical method for the solution of the fully elliptic, Reynolds-averaged Navier-Stokes equations has been used together with the $k$-$\varepsilon$ model of turbulence to examine the performance of three different treatments of the flow very close to a solid wall. The test cases selected include many features which are present in practical flows, including strong pressure gradients, surface curvatures, boundary layers and wakes, viscous-inviscid interaction, and separation. The results indicate that a two-layer approach, which combines a simpler one-equation model for the near-wall flow with the two-equation, $k$-$\varepsilon$ model for the flow beyond the wall layer, is quite successful in economically resolving the most important features of such flows. Its relative simplicity is attractive because additional modifications and generalizations for such factors as curvature, suction, blowing, wall roughness, unsteadiness, and three-dimensionality can be made. Accurate resolution of the flow in the near-wall region through the solution of the continuity and momentum equations, with a simple but realistic turbulence model, is, we believe, an important first step in the solution of complex three-dimensional flows. The two-layer model has been employed by Richmond and Patel[14] in a detailed investigation concerning the effects of pressure gradients and surface curvatures in two-dimensional turbulent flows.

From a computational perspective, the two-layer model is easier to implement, with a relatively few grid points in the wall layer, than the low-Reynolds-number models reviewed in Ref. 1. The two-layer approach is quite insensitive to grid spacing and the number of grid points in the inner layer, and to the location of the match boundary between the one- and two-equation models of the inner and outer layers. It is expected that other model combinations can be incorporated in such a two-layer scheme.

The present numerical scheme did not experience any special difficulty with the low-Reynolds-number model of Lam and Bremhorst when it was incorporated after the two-layer solution had converged. However, some earlier calculations, in which the model was employed from the beginning of the solution procedure, had indicated a tendency for breakdown. While this may be regarded as confirmation of the experience of other investigators, who have reported the need for many more grid points in the near-wall layer, grid sensitivity, and slow convergence of the solutions, we have not yet investigated the numerical details of that model thoroughly enough to provide a rigorous explanation. However, it appears to us that the two-layer model outperforms the low-Reynolds-number model, both from a numerical as well as a physical viewpoint.

## Acknowledgment

This research was supported by the Office of Naval Research under the Accelerated Research Initiative (Special Focus) Program in Ship Hydrodynamics, Contract N00014-83-K-0136.

## References

[1]Patel, V. C., Rodi, W., and Scheuerer, G., "Turbulence Models for Near-Wall and Low Reynolds Number Flows: A Review," *AIAA Journal*, Vol. 23, 1985, pp. 1308–1319.

[2]Patel, V. C. and Chen, H. C., "Turbulent Wake of a Flat Plate," *AIAA Journal*, Vol. 25, Aug. 1987, pp. 1078–1085.

[3]Chen, H. C. and Patel, V. C., "Calculation of Trailing-Edge, Stern and Wake Flows by a Time-Marching Solution of the Partially-Parabolic Equations," Iowa Institute of Hydraulic Research, University of Iowa, Iowa City, IIHR Rept. 285, 1985, revised 1987.

[4]Patel, V. C. and Chen, H. C., "Flow Over Tail and in Wake of Axisymmetric Bodies: Review of the State of the Art," *Journal of Ship Research*, Vol. 30, Sept. 1986, pp. 201–214.

[5]Lam, C. K. G. and Bremhorst, K. A., "Modified Form of the $k$-$\varepsilon$ Model for Predicting Wall Turbulence," *Transactions of the ASME, Journal of Fluids Engineering*, Vol. 103, Sept. 1981, pp. 456–460.

[6]Wolfshtein, M., "The Velocity and Temperature Distribution in One-Dimensional Flow with Turbulence Augmentation and Pressure Gradient," *International Journal of Heat & Mass Transfer*, Vol. 12, March 1969, pp. 301–318.

[7]Huang, T. T., Groves, N. C., and Belt, G., "Boundary-Layer Flow on an Axisymmetric Body with an Inflected Stern," David W. Taylor Naval Ship Research and Development Center, Bethesda, MD, Rept. 80-064, 1980.

[8]Huang, T. T., Wang, H. T., Santelli, N., and Groves, N. C., "Propeller/Stern/Boundary-Layer Interaction on Axisymmetric Bodies: Theory and Experiment," David W. Taylor Naval Ship Research and Development Center, Bethesda, MD, Rept. 76-0113, 1976.

[9]Patel, V. C., "A United View of the Law of the Wall Using Mixing-Length Theory," *Aeronautical Quarterly*, Vol. 24, Feb. 1973, pp. 55–70.

[10]Rodi, W. Celik, I., Demuren, A. O., Scheurerer, G., Shirani, I., Leschziner, M. A., and Rastogi, A. K., *Proceedings of the 1980–81 AFOSR-HTTM-Stanford Conference on Complex Turbulent Flows*, Vol. III, Stanford University, Stanford, CA, 1982, p. 1495.

[11]Launder, B. E., "Low-Reynolds-Number Turbulence Near Walls," University of Manchester Institute of Science and Technology, Thermo-Fluids Division, Rept. TFD/86/4, 1986.

[12]Patankar, S. V., *Numerical Heat Transfer and Fluid Flows*, McGraw-Hill, New York, 1980.

[13]Rodi, W. and Scheuerer, G., "Scrutinizing the $k$-$\varepsilon$ Turbulence Model Under Adverse Pressure Gradient Conditions," *Transactions of the ASME, Journal of Fluids Engineering*, Vol. 108, June 1986, pp. 174–179.

[14]Richmond, M. C., and Patel, V. C., "Pressure Gradient and Surface Curvature Effects in Turbulent Boundary Layers," AIAA Paper 87-1301, June 1987.